

What is measured by hyper-Rayleigh scattering from a liquid?

Micheal B. Rodriquez^{1,2} and David P. Shelton^{1,a)}

¹*Department of Physics and Astronomy, University of Nevada, Las Vegas, Nevada 89154-4002, USA*

²*Department of Physics and Astronomy, University of Rochester, Rochester, New York 14627-0171, USA*

(Received 8 November 2017; accepted 14 March 2018; published online 3 April 2018)

Polarization and angle dependence of hyper-Rayleigh scattering (HRS) measured for liquid acetonitrile and dimethyl sulfoxide (DMSO) is analyzed in terms of contributions from randomly oriented molecules and additional contributions produced during intermolecular collisions and induced by the electric field of dissolved ions. All three contributions show the effect of long-range correlation, and the correlation functions are determined using the HRS observations combined with the results of molecular dynamics simulations. HRS from acetonitrile is polarized transverse to the scattering vector. This is due to long-range molecular orientation correlation produced by the dipole-dipole interaction, and correlation at distances $r > 100$ nm must be included to account for the HRS observations. Analysis of the HRS measurements for acetonitrile determines the length scale $a = 0.185$ nm for the long-range longitudinal and transverse orientation correlation functions $B_L = -2B_T = a^3/r^3$. Transverse polarized collision-induced HRS is also observed for acetonitrile, indicating long-range correlation of intermolecular modes. Strong longitudinal HRS is induced by the radial electric field of dissolved ions in acetonitrile. For DMSO, the angle between the molecular dipole and the vector part of the first hyperpolarizability tensor is about 100° . As a result, HRS from the randomly oriented molecules in DMSO is nearly unaffected by dipole correlation, and ion-induced HRS is weak. The strong longitudinal polarized HRS observed for DMSO is due to the collision-induced contribution, indicating long-range correlation of intermolecular modes. The HRS observations require correlation that has r^{-3} long-range asymptotic form, for molecular orientation and for intermolecular vibration and libration, for both acetonitrile and DMSO. *Published by AIP Publishing.* <https://doi.org/10.1063/1.5012901>

I. INTRODUCTION

Second-harmonic or hyper-Rayleigh scattering (HRS) is a nonlinear light scattering technique widely used to measure the first hyperpolarizability β of molecules in solution,^{1,2} and HRS has largely replaced the previous alternative electric-field-induced second harmonic generation (ESHG or EFISH) technique.³ It is usually assumed that only incoherent scattering from the individual molecules contributes to HRS, and this is a good approximation for the contribution of a strong nonlinear optical chromophore in dilute solution, but it is not a good approximation for the solvent itself. The intensity, angle, and polarization dependence for incoherent HRS is modified by molecular orientation correlation extending to long range in the liquid.⁴⁻⁹ Fluctuations in β due to intermolecular interactions produce an additional spectral contribution [collision-induced (CI) wing], wider than the spectral component due to reorientation, and of comparable intensity.⁹⁻¹⁴ The dissolved ions in polar solvents also produce a coherent ESHG contribution with a narrow spectrum, which is due to the orientation correlations induced by the electric field of the ions in solution.^{15,16} Some or all of these overlapping spectral contributions may fall within the frequency band for HRS measurements, which is determined by the laser spectral width and the scattered light

spectral filter employed in the measurement. Lasers producing fs pulses with spectral width >100 cm^{-1} are often used for HRS experiments since the high peak power gives a large HRS signal. In this case, all three contributions are summed in the measurement. The analysis often considers only the incoherent individual molecule contribution, and this will lead to errors for the hyperpolarizability of the solvent molecules and for hyperpolarizabilities determined by the internal reference method, where the solvent hyperpolarizability is used for calibration.² In polar liquids, there is often an extrinsic ion-induced contribution due to ionic contamination, which is difficult to avoid or remove, and there is also an intrinsic ion-induced contribution in liquids such as water or ionic liquids that dissociate into ions.

All the above-mentioned effects enter the quantitative relation between molecular hyperpolarizability and HRS intensity, and the effects of correlation are distinctly different for the HRS contributions from the irreducible first rank (vector) and third rank (octupolar) parts of the third rank hyperpolarizability tensor β . Recently, theoretical expressions have been developed which account for HRS including the effects of ion-induced¹⁵ and intrinsic orientation correlation⁸ in dipolar liquids. One of the aims of the present work is to test these expressions which show that vector β with long-range orientation correlation produces HRS with different intensities for components polarized parallel [longitudinal (L)] or perpendicular [transverse (T)] to the scattering wavevector.

^{a)}shelton@physics.unlv.edu

HRS intensity from vector β can be expressed in terms of correlation functions for lab-frame components of the molecule-fixed vectors on pairs of molecules.⁸ In a homogeneous, isotropic liquid, the orientation correlation between unit vectors on pairs of molecules is a tensor function of the intermolecular displacement vector. This correlation tensor is diagonal in the coordinate frame with one axis aligned along the intermolecular vector, where the unit vector on each molecule has one longitudinal component (projection onto the intermolecular vector) and two transverse components (in the plane perpendicular to the intermolecular vector). The average products of corresponding longitudinal or transverse components of the two molecular unit vectors are the longitudinal (L) or transverse (T) orientation correlation functions, which are scalar functions of the intermolecular distance. The intensity of vector HRS as a function of the scattering wavevector is given by the spatial Fourier transform of this correlation tensor. The resulting spectral tensor is diagonal in the frame aligned with the scattering vector, with diagonal components longitudinal and transverse with respect to the scattering vector. The L and T spectral components produce HRS with distinctively different polarization and angle dependence. Expressing the L and T components of the spectral tensor in terms of the L and T components of the correlation tensor, one can show that unequal intensity for the L and T spectral components is the result of long-range orientation correlation. Dissection of the HRS spectrum into its L and T contributions is the main experimental result of this work.

Two dipolar liquids, acetonitrile and dimethyl sulfoxide (DMSO), are studied in the present work. In dipolar liquids, the dipole-dipole interaction results in long-range molecular orientation correlation, and theory predicts that this correlation in all cases produces a transverse HRS spectrum. Transverse HRS is observed for acetonitrile, in agreement with the theory, whereas longitudinal HRS is observed for DMSO, apparently contradicting the theory. This study seeks to understand the origin of longitudinal HRS from DMSO. The angle between the dipole and β vectors is not uniquely determined by symmetry in DMSO, and this angle affects the coherent HRS contribution and may also account for much weaker ion-induced HRS observed in DMSO than in acetonitrile. This study examines the quantitative accuracy of the theory for ion-induced HRS for both liquids. A broad collision-induced spectral wing makes another large contribution to the HRS intensity. This spectral wing results from rapid fluctuations induced by short-range intermolecular interactions, and in previous studies, it has been assumed that the intermolecular vibrations and librations mediated by these short-range interactions are local.^{9–14} However, hyper-Raman spectra have demonstrated that intra-molecular vibrational modes in liquids and glasses are non-local,^{17–19} and the present work finds evidence that the inter-molecular modes contributing to the collision-induced HRS spectrum are non-local as well.

In the following, the experimental methods are described and the experimental results are presented. Then the theoretical expressions for the angle and polarization dependence of intrinsic and ion-induced HRS are presented, followed by

analysis and discussion of the results. The results of molecular dynamics (MD) simulations for the liquids are used in the analysis.

II. HRS EXPERIMENT

The HRS experimental apparatus and methods are similar to those previously employed^{5,7,15,16,20–22} and are described and discussed in detail in Ref. 21. Linearly polarized pulses from an injection-seeded single-longitudinal-mode Nd:YAG (yttrium aluminium garnet) laser (operating at $\lambda_0 = 1064$ nm, 4.3 kHz repetition rate, 100 ns pulse duration) are focused to a 4.5 μm beam waist radius in the liquid sample. Scattered light is collected and collimated by an aspheric lens ($f = 13.8$ mm), analyzed by a linear polarizer, focused into an optical fiber, and fiber-coupled to a spectral filter or spectrometer followed by the photon counting detector. The sample temperature was $T = 25.0$ °C, and the laser beam average power in the sample was typically $P_{\text{av}} = 1.5$ W for acetonitrile and 2 W for DMSO-d6. Strong thermal lens effects due to absorption of the laser beam by overtone H stretching vibrations in DMSO are avoided by using DMSO-d6.

The acetonitrile (CH_3CN , 99.98%, Aldrich) and DMSO-d6 ($(\text{CD}_3)_2\text{SO}$, 99.9 at. % D, Aldrich) samples were de-ionized by continuous flow in a closed loop containing a PTFE (polytetrafluoroethylene)-tube peristaltic pump, an ion-exchange resin column (Dowex Monosphere MR-450 UPW), a 0.2 μm PTFE filter, a sample cell, a conductivity cell, and a reservoir, in that order. Samples with controlled, larger ion concentration were obtained by adding LiClO_4 (>99%, Fluka) or KClO_4 (>99%, Aldrich) to the de-ionized circulating fluid, with the ion-exchange column by-passed. The ion concentration was determined from the measured conductivity using the published results for LiClO_4 - CH_3CN and KClO_4 - $(\text{CH}_3)_2\text{SO}$ solutions.^{23,24} The de-ionized sample conductivity was typically in the range 1–5 nS/cm (estimated ion concentration 6–30 nM) for acetonitrile and 3–6 nS/cm (estimated ion concentration 75–150 nM) for DMSO-d6.

HRS measurements were made with linearly polarized light at scattering angles θ_s in the range from 0° to 180°. The sample cell was either a special 8-window cell for 45°, 90°, or 135° measurements or a standard square 10 mm fluorimeter cuvette for measurements at or near $\theta_s = 0^\circ$, 90°, or 180°. The laser beam was normally incident on the entrance window in all cases, but off-normal incidence at the exit window of the cuvette was required for some of the measurements. Scattering configurations with incident and scattered light polarized either perpendicular or parallel to the horizontal scattering plane are denoted VV, HV, VH, and HH, where V denotes the vertical polarization, H denotes the horizontal polarization, and the first and second letters refer to the incident and scattered light, respectively. Ratios of HRS intensities were measured ($I_{\text{VV}}/I_{\text{HV}}$, $I_{\text{HV}}/I_{\text{VH}}$, and $I_{\text{HH}}/I_{\text{VH}}$). The effect of intensity drift was canceled by using several hundred alternate 10 s measurements of the two polarization configurations for each ratio. Rapid switching between polarization configurations was enabled

using a liquid crystal variable wave plate (LCVWP) to control the laser polarization and a fast rotator²² to control the analyzing polarizer for the scattered light. The collection numerical aperture ($NA = n \sin \theta$) was controlled by a circular aperture following the collection lens, and the HRS intensity ratio at $NA = 0$ was obtained by extrapolating measurements in the range $0.04 < NA < 0.11$, made using several apertures, to zero collection aperture. Ratios were corrected for polarization dependent reflection at non-normal incidence.

The main HRS polarization ratio measurements were made with an interference filter selecting a 60 cm^{-1} spectral band (2 nm full width at half maximum, FWHM), centered on the 532 nm second-harmonic wavelength. Since the ion-induced HRS signal is difficult to eliminate, it was separately measured and then subtracted. The ion-induced HRS contribution was measured by inserting a fiber-coupled confocal Fabry–Pérot interferometer (10 cm mirror spacing, 750 MHz free spectral range) and scanning the spectrum with 13 MHz resolution. The spectral broadening of the ion-induced HRS signal due to the diffusive motion of the ions is typically $< 1 \text{ MHz}$, as compared to spectral broadening $> 30 \text{ GHz}$ for the other components of the HRS spectrum, so the ion-induced signal appears as a sharp spike riding on the flat background produced by the multiple overlapping orders of the much broader HRS spectrum. The relative ion-induced contribution is given by the ratio of integrated intensities for the spike and background in the Fabry–Pérot spectrum. Typically, 10^4 alternate scans of the reference spectrum (laser second-harmonic produced by a potassium titanyl phosphate [KTP] crystal) and the HRS spectrum were recorded, where the reference scans were used to lock the center of the Fabry–Pérot scans to the laser second-harmonic and to provide the instrument response function used for de-convolution of the ion-induced HRS spectrum.

Additional HRS polarization measurements were made at 90° scattering angle with $NA = 0.15$, using a wider filter to select a 336 cm^{-1} spectral band (9.5 nm FWHM, 532 nm center wavelength) and also using a fiber-coupled grating spectrometer (Jobin-Yvon Ramanor tandem, 1 m focal length, 1800 groove/mm gratings) to select a 2 cm^{-1} or 8 cm^{-1} spectral band. The spectrometer is polarization sensitive, so accurate HRS polarization measurements require an effective depolarizer placed before the spectrometer. The length scale for polarization mode mixing in a step index optical fiber is about 10 m,^{25,26} so the 2 m long spectrometer input fiber only partially depolarizes the light. The residual output polarization with linear polarized input light is measured by $r = I_{\max}/I_{\min}$, the ratio of maximum and minimum intensity transmitted through a linear polarizer placed at the fiber output. For the 2 m long, $200 \mu\text{m}$ core fiber, $r < 1.15$ was measured. A micro-patterned liquid crystal polymer depolarizer (Thorlabs DPP25-A) was placed after the fiber, and for this depolarizer, $r < 1.15$ was measured. For the combination of optical fiber followed by a micro-patterned depolarizer, $r < 1.01$ was measured, so the error in $I_{\text{HV}}/I_{\text{VH}}$ measurements due to the polarization sensitivity of the spectrometer was less than 1%.

III. HRS RESULTS

Measurements of the HRS intensity ratios $I_{\text{VV}}/I_{\text{HV}}$, $I_{\text{HV}}/I_{\text{VH}}$, and $I_{\text{HH}}/I_{\text{VH}}$ versus scattering angle θ_s in the horizontal plane are given in Table I for acetonitrile and Table II for DMSO-d6 and are plotted in Fig. 1. The measurements have been corrected for the ion-induced HRS contribution and extrapolated to zero collection aperture. Photon counting statistics account for the stated error bars on most of the data points. The expressions fit to the HRS intensity ratio data in Fig. 1 are⁷⁻⁹

$$I_{\text{VV}} = A_0 P^2 + A_T R^2, \quad (1)$$

$$I_{\text{HV}} = A_0 + A_T, \quad (2)$$

$$I_{\text{VH}} = A_0 + A_T \sin^2(\theta_s/2) + A_L \cos^2(\theta_s/2), \quad (3)$$

$$I_{\text{HH}} = A_0 [\sin^2 \theta_s + P^2 \cos^2 \theta_s] \\ + A_T [1 - (R - 1) \cos \theta_s]^2 \sin^2(\theta_s/2) \\ + A_L [1 + (R - 1) \cos \theta_s]^2 \cos^2(\theta_s/2), \quad (4)$$

where A_0 , A_T , and A_L are the intensity coefficients for HRS with the polarization and angle dependence for uncorrelated molecules (A_0) or for molecules with vector orientation correlation (A_T , A_L). Predominantly transverse HRS with $A_T > A_L$

TABLE I. HRS intensity ratio measurements versus scattering angles for CH_3CN at $T = 25^\circ\text{C}$. The HRS intensities are measured in a 60 cm^{-1} band and have been corrected for the ion-induced HRS contribution (1 S.D. uncertainty in the last digit is shown in parentheses).

θ_s (deg)	$I_{\text{VV}}/I_{\text{HV}}$	$I_{\text{HV}}/I_{\text{VH}}$	$I_{\text{HH}}/I_{\text{VH}}$
18.4	7.80(3)	5.28(18)	2.22(10)
45.0	7.79(2)	3.520(14)	1.089(4)
71.7	7.78(3)	2.202(6)	0.503(2)
78.9	7.69(3)	1.990(10)	0.596(4)
87.2 ^a			0.865(5)
90.0	7.76(3)	1.726(5)	0.988(2)
90.2 ^a	7.70(1)	1.725(8)	1.012(3)
93.2 ^a			1.173(4)
101.1	7.72(3)	1.514(5)	1.694(7)
108.4	7.75(3)	1.395(9)	2.286(16)
135.0	7.74(3)	1.143(3)	4.974(17)

^aFrom Ref. 5.

TABLE II. HRS intensity ratio measurements versus scattering angles for $(\text{CD}_3)_2\text{SO}$ at $T = 25^\circ\text{C}$. The HRS intensities are measured in a 60 cm^{-1} band and have been corrected for the ion-induced HRS contribution (1 S.D. uncertainty in the last digit is shown in parentheses).

θ_s (deg)	$I_{\text{VV}}/I_{\text{HV}}$	$I_{\text{HV}}/I_{\text{VH}}$	$I_{\text{HH}}/I_{\text{VH}}$
16.6	6.000(21)	0.473(2)	7.058(8)
45.0	6.001(11)	0.508(1)	4.608(16)
73.4	6.005(20)	0.577(2)	1.845(6)
87.3 ^a			1.084(1)
90.0	6.007(14)	0.635(3)	1.002(3)
90.0 ^a	6.047(12)	0.637(1)	0.994(2)
92.7 ^a			0.946(1)
106.6	5.990(17)	0.707(2)	1.047(5)
135.0	6.027(15)	0.864(2)	3.066(8)

^aFrom Ref. 5.

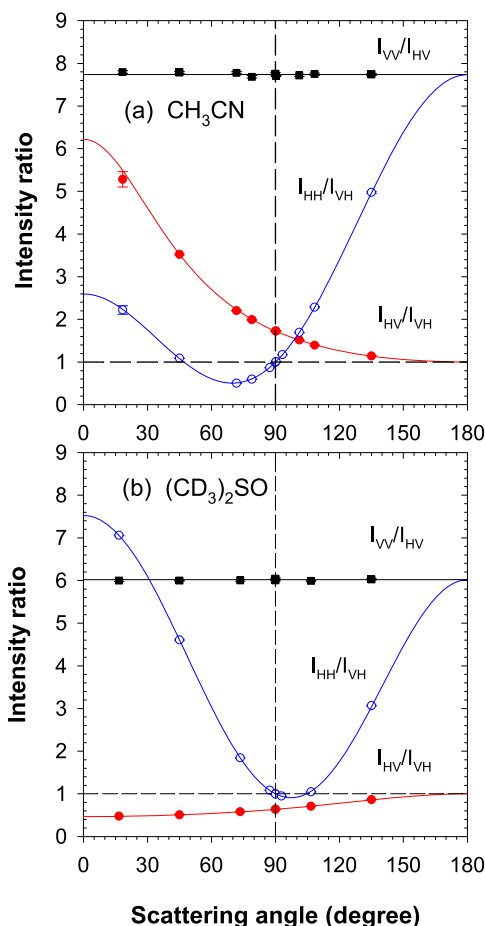


FIG. 1. Scattering angle dependence of HRS intensity ratio measurements (symbols) is compared to theoretical functions (curves) for (a) CH_3CN and (b) $(\text{CD}_3)_2\text{SO}$. The curves are obtained by fitting Eqs. (1)–(4) to (a) the data in Table I for CH_3CN , with fit parameters $P^2 = 2.59 \pm 0.04$, $R = 2.953 \pm 0.005$, $A_T/A_0 = 5.22 \pm 0.07$, and $A_L/A_0 = 0$, and (b) the data in Table II for $(\text{CD}_3)_2\text{SO}$, with fit parameters $P^2 = 6.020 \pm 0.011$, $R = 2.974 \pm 0.006$, $A_T/A_0 = 0$, and $A_L/A_0 = 1.137 \pm 0.006$. Correlations produce predominantly transverse HRS for CH_3CN and longitudinal HRS for $(\text{CD}_3)_2\text{SO}$. In the absence of correlations, the curves would be symmetric about 90° with $I_{\text{HV}}/I_{\text{VH}} = 1$ (dashed lines).

is indicated by polarization ratio $I_{\text{HV}}/I_{\text{VH}} > 1$, and longitudinal HRS with $A_T < A_L$ is indicated by $I_{\text{HV}}/I_{\text{VH}} < 1$. The fit parameters are $P^2 = 2.59 \pm 0.04$, $R = 2.953 \pm 0.005$, $A_T/A_0 = 5.22 \pm 0.07$, and $A_L/A_0 = 0$ for CH_3CN , and the fit parameters are $P^2 = 6.020 \pm 0.011$, $R = 2.974 \pm 0.006$, $A_T/A_0 = 0$, and $A_L/A_0 = 1.137 \pm 0.006$ for $(\text{CD}_3)_2\text{SO}$. Since sums of terms with $A_T = A_L$ have polarization and angle dependence identical to those of the A_0 terms and can be incorporated into the A_0 terms, the fitted curves obtained using Eqs. (1)–(4) are invariant for changes to alternative parameters P'^2 , A'_T/A'_0 , A'_L/A'_0 , where⁷

$$\frac{R^2 - P'^2}{R^2 - P^2} = \frac{1 + A'_T/A'_0}{1 + A_T/A_0} = \frac{1 + A'_L/A'_0}{1 + A_L/A_0}. \quad (5)$$

The curves in Fig. 1 are a good fit to the data and show that HRS is predominantly transverse for CH_3CN and longitudinal for $(\text{CD}_3)_2\text{SO}$. The transverse and longitudinal intensity coefficients, A_T and A_L , account for coherent HRS from that part of the third-rank first hyperpolarizability tensor β which transforms as a vector and is affected by long-range orientation correlation of the molecules.

The ion-induced HRS that has been removed from the data in Fig. 1 is the longitudinal contribution to the coherent HRS intensity produced when dipolar molecules surrounding an ion are oriented by the radial electric field of the ion. Measurements of this ion-induced HRS signal are shown in Fig. 2 for acetonitrile and in Fig. 3 for DMSO- d_6 . Figure 2(a) shows $I_{\text{HV}}/I_{\text{VH}}$ measured for LiClO_4 - CH_3CN solutions as a function of ionic strength $c = (1/2) \sum_i Z_i^2 \rho_i$, where Z_i is the charge and ρ_i is the concentration of ion species i . Figure 3(a) shows $I_{\text{HV}}/I_{\text{VH}}$ measured for KClO_4 - $(\text{CD}_3)_2\text{SO}$ solutions. Ion-induced HRS is much weaker for DMSO- d_6 than for acetonitrile, so the DMSO- d_6 measurements were made at 16.6° to increase the ion-induced HRS signal. The curves fit to the data points in Figs. 2(a) and 3(a) have the form¹⁵

$$I_{\text{HV}}/I_{\text{VH}} = A/[1 + Bx/(1 + x)], \quad (6)$$

where $x = c/c_0$, $A = (I_{\text{HV}}/I_{\text{VH}})_{c=0}$, and $B = (I_{\text{VH}}^i)_{c \rightarrow \infty} / (I_{\text{VH}})_{c=0} = I_{\text{VH},\infty}^i / I_{\text{VH},0}$. Equation (6) is the ratio of HRS intensity I_{HV} , which is independent of ion concentration, and

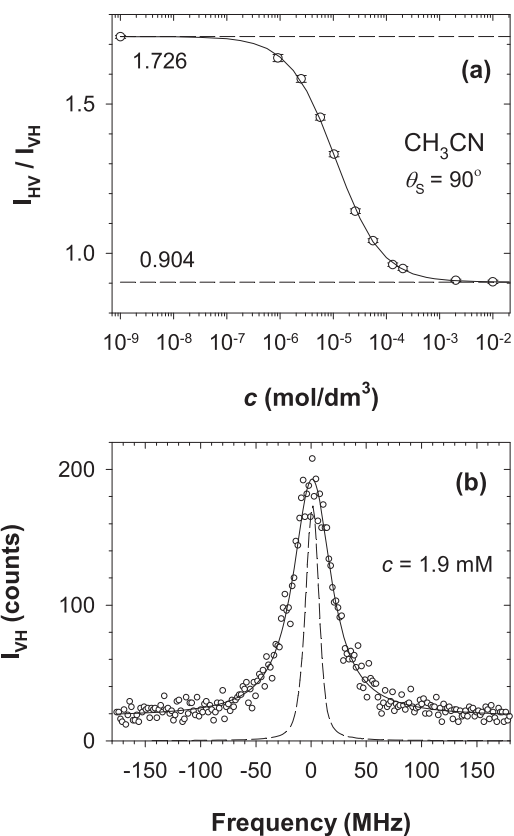


FIG. 2. (a) HRS intensity ratio $I_{\text{HV}}/I_{\text{VH}}$ at 90° scattering angle for LiClO_4 - CH_3CN solutions measured as a function of ionic strength c . The solid curve shows the fit of Eq. (6) to the data (open circles), with fit parameters $c_0 = 21.1 \pm 0.5 \mu\text{M}$, $A = 1.726 \pm 0.004$, and $B = 0.910 \pm 0.004$. The dashed lines show the low and high concentration limiting values for the ratio, 1.726 and 0.904, respectively. The ion-induced HRS contribution must be eliminated or subtracted to measure HRS intrinsic to the solvent. The data point plotted at 1 nM was obtained by measuring and correcting for the residual ion spike in a de-ionized sample. (b) Fabry-Pérot scan of the VH HRS spectrum for a 2.0 mM LiClO_4 - CH_3CN solution (data, open circles; fit, solid curve; scaled down KTP SHG reference, dashed curve). At this high ion concentration, the relative integrated intensity of the ion-induced spike and the broad intrinsic HRS background is 0.88 ± 0.04 and the width of spike is $16.0 \pm 0.6 \text{ MHz}$ (HWHM, de-convolved Lorentzian).

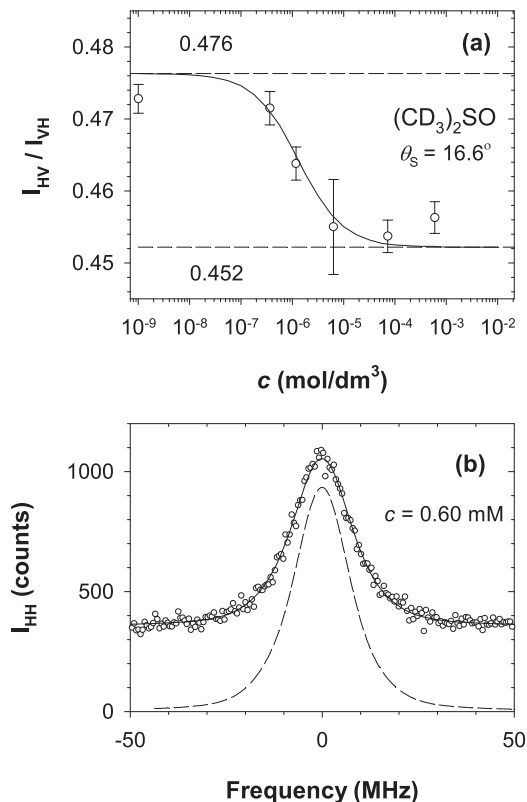


FIG. 3. (a) HRS intensity ratio I_{HV}/I_{VH} at 16.6° scattering angle for KClO_4 – $(\text{CD}_3)_2\text{SO}$ solutions measured as a function of ionic strength c . The solid curve shows the fit of Eq. (6) to the data (open circles), with fit parameters $c_0 = 1.38 \mu\text{M}$, $A = 0.4763 \pm 0.0013$, and $B = 0.0533$. The dashed lines show the low and high concentration limiting values for the ratio, 0.476 and 0.452, respectively. The data point plotted at 1 nM was obtained by measuring and correcting for the residual ion spike in a de-ionized sample. (b) Fabry–Pérot scan of the HH HRS spectrum for a 0.60 mM KClO_4 – $(\text{CD}_3)_2\text{SO}$ solution (data, open circles; fit, solid curve; scaled down KTP SHG reference, dashed curve). At this high ion concentration, the relative integrated intensity of the ion-induced spike and the broad intrinsic HRS background is 0.0630 ± 0.0014 and the width of spike is 0.84 ± 0.17 MHz (HWHM, de-convolved Lorentzian).

$I_{VH} = I_{VH,0} + I_{VH}^i$, which has an ion-induced contribution I_{VH}^i that saturates at high ion concentration. The ion-induced HRS contribution I_{VH}^i is determined more accurately from the ratio I_{HV}/I_{VH} because I_{HV} serves as an ion-independent internal reference for the measurements of the ion concentration dependent intensity I_{VH} . The polarization and angle dependence for ion-induced HRS is given by $I_{VV}^i = I_{HV}^i = 0$,^{9,15}

$$I_{VH}^i = \frac{2x \cos^2(\theta_s/2)}{2 \sin^2(\theta_s/2) + 2 \sin^2(\theta_0/2) + x} I_{VH,\infty,90}^i, \quad (7)$$

$$I_{HH}^i = [1 + (R - 1) \cos \theta_s]^2 I_{VH}^i, \quad (8)$$

where $I_{VH,\infty,90}^i$ is the maximum value for I_{VH}^i at $\theta_s = 90^\circ$, $2 \sin^2(\theta_0/2) = (n_i - n_s)^2 / (2n_i n_s)$, and n_i (n_s) is the liquid refractive index at the incident (scattered) wavelength ($\theta_0 = 0.15^\circ$ for acetonitrile and 0.33° for DMSO-d6). The ion-induced HRS spectrum at high ionic strength, measured using the confocal Fabry–Pérot interferometer, is shown in Fig. 2(b) for acetonitrile and in Fig. 3(b) for DMSO-d6 (with HH polarization to maximise the signal for DMSO-d6). The ion-induced HRS contribution relative to the intrinsic HRS contribution is simply determined from such spectra; it is given

by the integrated intensity ratio for the ion-induced peak and the flat intrinsic background in the spectrum. The ion-induced HRS contribution can be measured even at low ionic strength from such spectra. The ion-induced HRS intensity at low ionic strength, such that $x \ll 1$, is given by $I_{VH}^i \propto x / \tan^2(\theta_s/2)$ and is largest at small forward angles.

The ion-induced HRS contributions from residual ions in the de-ionized samples were subtracted to obtain the results plotted in Fig. 1. The residual ion-induced HRS contribution for acetonitrile in this work was $<1\%$ of the intrinsic HRS contribution for all scattering angles $>45^\circ$, $\approx 1\%$ for $\theta_s = 45^\circ$, and $\approx 10\%$ for $\theta_s = 18^\circ$. Although Fabry–Pérot scans were used to directly measure the ion-induced contribution, the accuracy of the correction for ion-induced HRS at $\theta_s = 18^\circ$ was limited by uncontrolled variations ≈ 10 nM in the residual ion concentration during those measurements. The residual ion-induced HRS corrections for DMSO-d6 were smaller, $<1\%$ at 16.6° and $<0.1\%$ at all larger scattering angles.

The third contribution to the measured HRS intensity is due to collision-induced inter-molecular HRS, which has a spectrum much wider than the orientational HRS spectrum that it overlaps.^{12–14} The intensity ratios I_{VV}/I_{HV} and I_{HV}/I_{VH} for just this HRS contribution can be determined from the differences of the HRS intensities measured with 60 and 336 cm^{-1} bandwidth (BW) filters, as shown in Table III. The collision-induced HRS for frequency shift $\Delta\nu > 30 \text{ cm}^{-1}$ is transverse for acetonitrile and longitudinal for DMSO-d6. This is shown by the polarization ratio $(I_{HV}/I_{VH})_{2-1}$ for $\Delta\nu > 30 \text{ cm}^{-1}$ in the last line of Table III, which is 1.46 for acetonitrile, indicating predominantly transverse HRS, and 0.50 for DMSO-d6, indicating predominantly longitudinal HRS. The intensity ratios at smaller frequency shift can be measured using the grating spectrometer to select the measurement spectral band. Table IV gives measurements with an 8 cm^{-1} band centered at 20 cm^{-1} shift which excludes the central orientational HRS component (partially for acetonitrile and completely for DMSO-d6). This measurement of collision-induced HRS is also transverse for acetonitrile and longitudinal for DMSO-d6. Also shown in Table IV are DMSO-d6 intensity ratios measured

TABLE III. HRS measurements for CH_3CN and $(\text{CD}_3)_2\text{SO}$ at 90° scattering angle, using both 60 and 336 cm^{-1} wide spectral filters (filter 1 and filter 2). The result $I_{VV,2}/I_{VV,1}$ is corrected for relative filter transmission at 532 nm, and subscript 2-1 denotes intensity difference results for the two filters (1 S.D. uncertainty in the last digit is shown in parentheses).

	Acetonitrile	DMSO-d6
$(I_{VV}/I_{HV})_1$	7.79(5)	5.97(3)
$(I_{HV}/I_{VH})_1$	1.680(7)	0.630(3)
$(I_{VV}/I_{HV})_2$	7.32(2)	5.28(3)
$(I_{HV}/I_{VH})_2$	1.580(4)	0.560(2)
$I_{VV,2}/I_{VV,1}$	1.60(2)	1.69(2)
$I_{HV,2}/I_{HV,1}$ ^a	1.71(2)	1.91(2)
$I_{VH,2}/I_{VH,1}$ ^b	1.81(3)	2.15(3)
$(I_{VV}/I_{HV})_{2-1}$ ^c	6.7(3)	4.5(2)
$(I_{HV}/I_{VH})_{2-1}$ ^d	1.46(7)	0.50(2)

^a $I_{HV,2}/I_{HV,1} = (I_{VV,2}/I_{VV,1})(I_{VV}/I_{HV})_1/(I_{VV}/I_{HV})_2$.

^b $I_{VH,2}/I_{VH,1} = (I_{HV,2}/I_{HV,1})(I_{HV}/I_{VH})_1/(I_{HV}/I_{VH})_2$.

^c $(I_{VV}/I_{HV})_{2-1} = (I_{VV}/I_{HV})_1(I_{VV,2}/I_{VV,1}-1)/(I_{HV,2}/I_{HV,1}-1)$.

^d $(I_{HV}/I_{VH})_{2-1} = (I_{HV}/I_{VH})_1(I_{HV,2}/I_{HV,1}-1)/(I_{VH,2}/I_{VH,1}-1)$.

TABLE IV. HRS measurements for CH₃CN and (CD₃)₂SO at 90° scattering angle, with 2 or 8 cm⁻¹ spectral bandwidth using the spectrometer (1 S.D. uncertainty in the last digit is shown in parentheses).

Liquid	$\Delta\nu$ (cm ⁻¹)	BW (cm ⁻¹)	I_{VV}/I_{HV}	I_{HV}/I_{VH}
Acetonitrile	20	8	5.19(17)	1.28(4)
DMSO-d6	20	8	3.79(8)	0.45(1)
DMSO-d6	0	2	8.16(17)	0.98(3)

in a narrow band (2 cm⁻¹) at 0 cm⁻¹ shift, which selects orientational HRS and effectively excludes collision-induced HRS for DMSO-d6. This measurement is consistent with incoherent orientational HRS ($I_{HV}/I_{VH} = 1$) and dominantly vector β ($I_{VV}/I_{HV} \approx 9$) for DMSO-d6.

Molecular hyperpolarizabilities are usually determined assuming incoherent HRS, using HRS relative intensity measurements for different samples in the same apparatus, where $I^{(2\omega)} \propto F\beta^2P^2$. The sample dependent factor F is^{27,28}

$$F = \rho L_{\omega}^4 L_{2\omega}^2 t_{\omega}^2 t_{2\omega} (1 - \alpha_{\omega})^2 (1 - \alpha_{2\omega}) n_{\omega} / n_{2\omega}^2, \quad (9)$$

where ρ is the molecular number density, $L = (n^2 + 2)/3$ is the Lorentz local field factor, $t = [1 - (n_w - n)^2 / (n_w + n)^2]$ is the Fresnel transmission factor, α is the sample absorption factor for the incident laser beam or the HRS light, and n (n_w) is the sample (window) refractive index. Molecular data and the calculated values for F are given in Table V. The absorption of the incident laser beam is $\alpha_{\omega} < 0.1\%$, which is negligible, but the thermal defocusing of the incident beam due to this absorption is not negligible. The effect of the thermal lens is eliminated by using $I^{(2\omega)}/P^2$ extrapolated to $P = 0$. Relative HRS intensity $[I_{\text{DMSO}}^{(2\omega)}/P^2]_{P=0} / [I_{\text{CH}_3\text{CN}}^{(2\omega)}/P^2]_{P=0} = 0.482 \pm 0.013$ is measured for DMSO-d6 and acetonitrile. The corresponding relative hyperpolarizability obtained using^{27,28}

$$\beta \propto [I_{\text{VV}}^{(2\omega)}/FP^2]^{1/2} \quad (10)$$

is $\beta_{\text{DMSO}}/\beta_{\text{CH}_3\text{CN}} = 0.640 \pm 0.010$, slightly smaller for DMSO-d6 than for acetonitrile.²⁸ A better estimate would account for orientation correlation and other spectral components included in the measured intensity.

TABLE V. Molecular data and derived quantities for liquid CH₃CN and (CD₃)₂SO at $T = 25$ °C (references in square brackets).

	Acetonitrile	DMSO-d6
ρ (M)	18.93 [23]	14.08 [24]
$n(1064 \text{ nm})$	1.3354 [47]	1.4638 [47]
$n(532 \text{ nm})$	1.3422 [48]	1.4809 [49]
$F(\text{M})^a$	56.70	66.75
μ (D)	4.5 [37]	4.10 [40]
y^b	7.826	4.832
ϵ_s	35.96 [50]	46.48 [51]
ϵ_{∞}	3.33 [50]	4.16 [51]
$f(0)$	2.547	2.948
B_0^c	2.118	1.355

^aEquation (9) using $n_w(1064 \text{ nm}) = 1.4496$ and $n_w(532 \text{ nm}) = 1.4607$ for fused silica.

^bEquation (14).

^cEquation (44).

IV. DIPOLE CORRELATION FROM MOLECULAR DYNAMICS SIMULATION

Molecular dynamics (MD) simulations for each liquid provide information about molecular correlations needed to go beyond the incoherent approximation in the analysis of the HRS observations. In particular, the observed HRS polarization and angle dependence can be explained by long-range orientation correlation of the molecular dipole vectors and the vector part of the β hyperpolarizability tensor.⁸ Molecular dynamics simulations were performed using the GROMACS software package (version 5.1.4).²⁹ All-atom, non-polarizable molecules were simulated in a cubic box with periodic boundary conditions; long-range Coulomb interactions were treated by the particle mesh Ewald (PME) method with conducting boundary conditions, while Lennard-Jones (LJ) 6-12 interactions were treated using a 1.0 nm cutoff radius and analytical dispersion correction.³⁰ Temperature and pressure were controlled using a modified velocity rescaling thermostat³¹ and a Berendsen barostat. Equilibrium density at $T = 298$ K and $p = 101$ kPa was determined using NPT simulations, while NVT simulations at the equilibrium density were used to

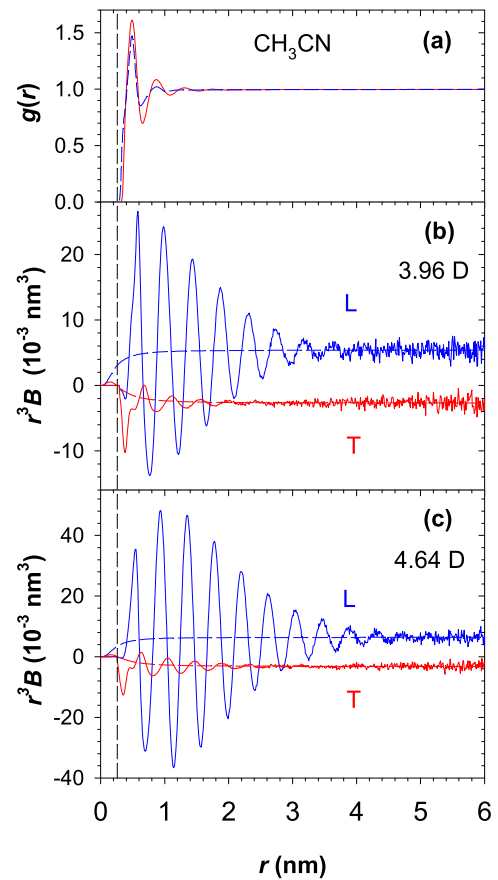


FIG. 4. (a) Radial pair distribution functions for acetonitrile from molecular dynamics simulations ($\mu = 3.96$ D, solid red; $\mu = 4.64$ D, dashed blue). Correlation functions for (b) $\mu = 3.96$ D and (c) $\mu = 4.64$ D, with longitudinal (blue curves) and transverse (red curves) orientation correlation functions from the MD simulations (solid curves), compared with functions given by Eqs. (25) and (26) with a from Eq. (18) given in Table VI (dashed curves). The vertical dashed line at 0.27 nm marks the boundary of the exclusion region for other molecules. Asymptotic functions $B \propto r^{-3}$ appear as horizontal lines in this graph.

determine the correlation functions. Simulations for acetonitrile with $N = 27\,000$ molecules in a 13.33 nm box were equilibrated for 2 ns before a 20 ns production run with 2 fs time steps. Simulations for DMSO with 8000 molecules in a 9.8 nm box were run for 2 ns with 2 fs time steps. Further details of the MD simulation models are given in the [supplementary material](#).

The full, longitudinal, and transverse dipole-dipole correlation functions computed from the simulation trajectory are^{32,33}

$$F(r) = \langle \hat{\mu}_i \cdot \hat{\mu}_j \rangle, \quad (11)$$

$$L(r) = \langle (\hat{\mu}_i \cdot \hat{r}_{ij})(\hat{\mu}_j \cdot \hat{r}_{ij}) \rangle, \quad (12)$$

$$T(r) = \frac{1}{2}[F(r) - L(r)], \quad (13)$$

where $\hat{\mu}_i$ is the dipole unit vector on molecule i and \hat{r}_{ij} is the unit vector in the direction from molecule i to j . Corrections $\delta F = 3\delta L = 3\delta T = -(\varepsilon - 1)^2/(9y\varepsilon N)$ ^{9,34,35} are applied to the MD simulation results to obtain results for an infinite homogeneous system, where³⁴

$$y = \rho\mu^2/(9\varepsilon_0k_B T) \quad (14)$$

is the dimensionless dipole strength, ρ is the molecular number density, and μ is the molecular dipole moment. The dielectric constant ε is calculated using the correlation function expression³⁴

$$g_K = 1 + 4\pi\rho \int F(r)g(r)r^2 dr \quad (15)$$

for the Kirkwood correlation factor g_K and then solving the Kirkwood relation³⁴

$$(\varepsilon - 1)(2\varepsilon + 1)/\varepsilon = 9yg_K \quad (16)$$

for ε . The correction is about $\delta L = -5 \times 10^{-6}$ (-4×10^{-5}) for the acetonitrile (DMSO) MD simulation. The correlation

functions at large r for a non-polarizable dipole fluid have the asymptotic values^{9,34}

$$L(r) = -2T(r) = a^3/r^3 \quad (17)$$

with the correlation strength parameter^{9,34}

$$a^3 = (\varepsilon - 1)^2/(18\pi y\varepsilon\rho). \quad (18)$$

The MD simulation results for acetonitrile correlation functions are shown in Fig. 4. The radial pair distribution function $g(r)$ plotted in Fig. 4(a) shows that other molecules are excluded for $r < 0.27$ nm and that position correlations vanish for $r > 2$ nm. The orientation correlation functions $r^3L(r)$ and $r^3T(r)$ plotted in Figs. 4(b) and 4(c) reach constant long-range limiting values for $r > 5$ nm, with limiting values in good agreement with the values calculated using Eqs. (17) and (18). The dipole moment of polarizable molecules in the liquid is larger than the gas phase molecular dipole. A combined Monte Carlo/quantum mechanical (QM) calculation finds that $\mu = 3.94$ D calculated for an isolated acetonitrile molecule is increased to 4.65 ± 0.19 D for a molecule in liquid acetonitrile,³⁶ consistent with $\mu = 4.5 \pm 0.1$ D obtained from a measurement of the integrated intensity of far-infrared absorption.³⁷ MD simulation results are shown for the two models, the first (MD1) with dipole moment near the measured gas phase value and the second (MD2) with dipole moment close to the measured liquid phase dipole. The correlation strength increases with the magnitude of the molecular dipole moment. MD simulation results for the two acetonitrile models are summarized in Table VI.

The MD simulation results for the DMSO dipole correlation functions shown in Fig. 5 are qualitatively similar to those for acetonitrile. In contrast to acetonitrile, the dipole vector direction for DMSO is not determined by symmetry, and the β vector may not be parallel to the dipole vector. The β vector correlations that result from the dipole correlations will

TABLE VI. MD simulation results for CH₃CN and (CH₃)₂SO. Asymptotic orientation correlation strength a^3 is calculated using Eq. (18), and the transverse (T) and longitudinal (L) spatial spectral intensities S_T and S_L are obtained by integrating the orientation correlation functions using Eqs. (21)–(24) and (29)–(31).

Model	CH ₃ CN MD1	CH ₃ CN MD2	DMSO $\theta_{\mu\beta} = 0^\circ$	DMSO $\theta_{\mu\beta} = 104^\circ$
ρ (nm ⁻³)	11.397	11.397	8.493	8.493
μ (D)	3.96	4.64	5.21	5.21
ε^a	22.7	35.7	65.7	65.7
y^b	6.0717	8.3358	7.836	7.836
a^3 (10 ⁻³ nm ³) ^c	5.30	6.28	16.92	1.60 ^d
a (nm)	0.1744	0.1845	0.2567	0.1170
$S_{T,1} = S_{L,1}$ (10 ⁻³ nm ³)	29.24	29.24	39.25	39.25
$S_{T,2} = S_{L,2}$ (10 ⁻³ nm ³)	-5.54	-1.80	33.29	-0.59
$S_{T,3}$ (10 ⁻³ nm ³)	10.75	13.21	35.79	3.36
$S_{L,3}$ (10 ⁻³ nm ³)	-22.55	-26.25	-70.54	-6.70
S_T (10 ⁻³ nm ³)	34.46	40.65	108.32	42.02
S_L (10 ⁻³ nm ³)	1.15	1.19	1.99	31.97
S_L/S_T	0.035	0.029	0.018	0.761
$C_T = S_T/S_{T,1}$	1.178	1.390	2.760	1.071
$C_L = S_L/S_{L,1}$	0.039	0.041	0.051	0.815

^aEquation (16).

^bEquation (14).

^cEquation (18).

^dEquation (18) $\times \cos^2\theta_{\mu\beta}$.

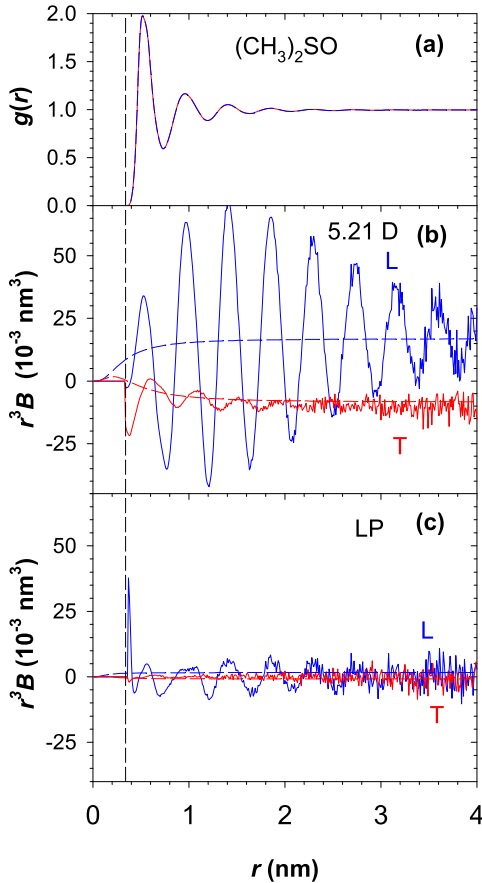


FIG. 5. (a) Radial pair distribution functions for DMSO from molecular dynamics simulations (solid blue). Correlation functions for (b) molecular dipole vector and (c) molecular lone pair vector, with longitudinal (blue curves) and transverse (red curves) orientation correlation functions from the MD simulations (solid curves), compared with functions (dashed curves) given by Eqs. (25) and (26). The vertical dashed line at 0.34 nm marks the boundary of the exclusion region for other molecules. Asymptotic functions $B \propto r^{-3}$ appear as horizontal lines in this graph.

be reduced by the projection factor $\cos^2\theta_{\mu\beta}$, where $\theta_{\mu\beta}$ is the angle between the dipole and β vectors. The DMSO dipole lies along the O-S bond,³⁸ and the β vector may lie in the direction of the S lone-pair. The angle $\theta_{\mu\beta} = 104^\circ$ is obtained from the MD simulation assuming that the β vector is in the direction of the S lone-pair, which is estimated as the direction given by the vector sum of the bond vectors for the C-S, C-S, and O-S bonds. Figure 5(c) shows the β vector orientation correlation functions calculated from the MD trajectory, for the β vector in the direction of the S lone-pair. The ratio of β correlation functions in Fig. 5(c) and the corresponding dipole correlation functions in Fig. 5(b), averaged over $0.5 < r < 2.5$ nm, is 0.10 ± 0.03 for the longitudinal correlations and 0.04 ± 0.04 for the transverse correlations, as compared to the projection factor $\cos^2\theta_{\mu\beta} = 0.06$ for $\theta_{\mu\beta} = 104^\circ$. MD simulation results for DMSO with $\theta_{\mu\beta} = 0^\circ$ and 104° are summarized in Table VI.

V. COHERENT HRS FROM DIPOLE ORIENTATION CORRELATION

The terms with intensity coefficients A_T and A_L in Eqs. (1)–(4) are due to vector β HRS for molecules with

long-range orientation correlations given by the transverse and longitudinal vector correlation functions $B_T(r)$ and $B_L(r)$. The intensity coefficients A_T and A_L are proportional to the diagonal components $S_T(K)$ and $S_L(K)$ of the spatial Fourier transform of the correlation tensor, given by the expressions^{8,9,33}

$$S_T(K) = 4\pi \int_0^\infty g(r)r^2 dr \left[\left\{ j_0(Kr) - \frac{j_1(Kr)}{Kr} \right\} B_T(r) + \frac{j_1(Kr)}{Kr} B_L(r) \right], \quad (19)$$

$$S_L(K) = 4\pi \int_0^\infty g(r)r^2 dr \left[2 \frac{j_1(Kr)}{Kr} B_T(r) + \left\{ j_0(Kr) - 2 \frac{j_1(Kr)}{Kr} \right\} B_L(r) \right], \quad (20)$$

where $j_n(x)$ are the spherical Bessel functions.

These integrals are evaluated piecewise over three regions,^{8,9,33}

$$S_T = S_{T,1} + S_{T,2} + S_{T,3}, \quad (21)$$

$$S_L = S_{L,1} + S_{L,2} + S_{L,3}. \quad (22)$$

The delta function self-correlation in region 1 ($r < r_1$, where r_1 is the radius of the excluded volume) gives⁸

$$S_{T,1} = S_{L,1} = (1/3)(4\pi r_0^3/3), \quad (23)$$

where $4\pi r_0^3/3 = \rho^{-1}$ is the volume per molecule. In region 2 ($r_1 < r < r_2$), the correlation functions $B_L(r) = L(r)$ and $B_T(r) = T(r)$ obtained from the MD simulation are integrated to give $S_{T,2}$ and $S_{L,2}$. At short range where $Kr \ll 1$, it is a good approximation to take the $K = 0$ limit for the integrand in Eqs. (19) and (20), which gives⁸

$$S_{T,2} = S_{L,2} = 4\pi \int_{r_1}^{r_2} r^2 dr g(r) [B_L(r) + 2B_T(r)]. \quad (24)$$

This integral also appears in Eq. (15) for g_K . The results in Table VI for acetonitrile (DMSO) are obtained using $r_1 = 0.27$ (0.34) nm and $r_2 = 5.0$ (4.5) nm.

The integrals for region 3 ($r > r_2$) are evaluated using the correlation functions^{8,9,33}

$$B_T(r) = [1 + (r/a)^2]^{-3/2} [1 - \frac{3}{2}r^2/(r^2 + a^2)], \quad (25)$$

$$B_L(r) = [1 + (r/a)^2]^{-3/2} \quad (26)$$

which give the correct asymptotic r^{-3} dependence and a solenoidal (zero divergence) vector field. Equations (19) and (20) with these correlation functions and $g(r) = 1$ give⁸

$$S_T(K) = 2\pi a^3 K a K_1(Ka), \quad (27)$$

$$S_L(K) = 0, \quad (28)$$

where $K_n(x)$ is the modified Bessel function of the second kind, of order n . Again taking the $K = 0$ limit, the integrals over region 3 ($r > r_2$) for these correlation functions are⁸

$$S_{T,3} = 2\pi a^3 - S_{TL,3}, \quad (29)$$

$$S_{L,3} = 0 - S_{TL,3}, \quad (30)$$

where

$$S_{TL,3} = 4\pi \int_0^{r_2} r^2 dr [B_L(r) + 2B_T(r)] = (4\pi a^3/3) [1 + (a/r_2)^2]^{-3/2}. \quad (31)$$

The contributions to Eqs. (21) and (22) from each region, and the totals for S_T and S_L , are given in Table VI for acetonitrile and DMSO. Orientation correlation affects S_T and S_L in two ways.³³ The first effect is that S_T and S_L differ from the incoherent HRS value $S_{T,1} = S_{L,1}$, by the intensity enhancement factors C_T and C_L given in Table VI. The second effect is that S_T and S_L are not equal. The second effect is entirely due to the long-range correlation in region 3, and it produces HRS polarization and angle dependence observably different from that for incoherent HRS. Orientation correlations due to the dipole-dipole interaction always produce transverse HRS with $S_L \leq S_T$.³³ Table VI shows $S_L \ll S_T$ for both acetonitrile models and for the DMSO model with $\theta_{\mu\beta} = 0^\circ$. Table VI shows $S_L \approx S_T$ for the DMSO model with $\theta_{\mu\beta} = 104^\circ$, and for $\theta_{\mu\beta} = 90^\circ$, the long-range correlation for vector β due to the dipole correlation will vanish, giving $S_L = S_T$. A value $\theta_{\mu\beta} > 90^\circ$ is indicated by liquid phase ESHG experiments which find $\gamma_{||} + \mu\beta_{||}/3k_B T$ is negative for DMSO.^{39,40}

HRS is mediated by the tensor β which is the direct sum of four irreducible spherical tensors⁴¹

$$\beta = \beta^{[ss,1]} \oplus \beta^{[ms,1]} \oplus \beta^{[ms,2]} \oplus \beta^{[ss,3]}, \quad (32)$$

where $\beta_m^{[\nu,l]}$ is a spherical tensor of rank l with $2l + 1$ components m , index ν labels the symmetry under permutation of the Cartesian tensor indices (ss is totally symmetric, while ms is non-symmetric for first index permutations), and the mixed symmetry $\nu = ms$ tensors vanish when Kleinman symmetry holds. Expressed in terms of spherical tensor components, the HRS intensities given by Eqs. (1)–(4) at $\theta_s = 90^\circ$ are⁴¹

$$\begin{aligned} I_{VV} &= R^2 A_T + P^2 A_0 \\ &= C_T \frac{9}{45} |\beta^{[ss,1]}|^2 + \frac{6}{105} |\beta^{[ss,3]}|^2, \end{aligned} \quad (33)$$

$$\begin{aligned} I_{HV} &= A_T + A_0 \\ &= C_T \frac{1}{45} |\beta^{[ss,1]}|^2 + \sqrt{5} \beta^{[ms,1]}|^2 + \frac{1}{15} |\beta^{[ms,2]}|^2 \\ &\quad + \frac{4}{105} |\beta^{[ss,3]}|^2, \end{aligned} \quad (34)$$

$$\begin{aligned} I_{VH} &= I_{HH} = \frac{1}{2}(A_T + A_L) + A_0 \\ &= (C_T + C_L) \frac{1}{90} |\beta^{[ss,1]}|^2 + \frac{1}{15} |\beta^{[ms,2]}|^2 \\ &\quad + \frac{4}{105} |\beta^{[ss,3]}|^2, \end{aligned} \quad (35)$$

where $|\beta^{[\nu,l]}|^2 = \sum_m |\beta_m^{[\nu,l]}|^2$. The β components with $l = 1$ transform as vectors under rotations, and $R^2 = (I_{VV}/I_{HV})_{l=1}$ is the HRS intensity ratio due to just these terms. Similarly, $P^2 = (I_{VV}/I_{HV})_{l=2,3}$ is the HRS intensity ratio due to just the terms with $l = 2$ and 3. Dipole orientation correlation affects only the $l = 1$ HRS contribution and is accounted for by the factors C_T and C_L . Short range quadrupolar and octupolar orientation correlation effects for the $l = 2$ and 3 terms are ignored since they can change the values for P^2 and A_0 , but not the polarization and angle dependence.

The coefficients A_0 , A_T , and A_L in Eqs. (33)–(35) will be directly comparable to the coefficients experimentally determined from the fits of Eqs. (1)–(4) to the HRS data in Fig. 1, provided that P^2 in the experimental fit includes only the

$l = 2$ and 3 contributions. The transformation to the set of fit coefficients with the correct value for P^2 is given by Eq. (5). The correct value is $P^2 = 3/2$ in the case that Kleinman symmetry holds so that the $l = 2$ contribution vanishes, but this is not true in general. However, for acetonitrile which has C_{3v} symmetry, the nonvanishing independent Cartesian tensor components are β_{zzz} , β_{zxx} , β_{xxz} , and β_{yyy} , and the $l = 2$ contribution vanishes by symmetry.⁴¹ Transforming the parameters for the acetonitrile HRS fit in Fig. 1(a) using Eq. (5) gives $P^2 = 1.500$, $R = 2.953 \pm 0.005$, $A_T/A_0 = 6.33 \pm 0.12$, and $A_L/A_0 = 0.179 \pm 0.008$. The ratio $A_L/A_T = 0.0282 \pm 0.0014$ for these fit coefficients is directly comparable with the MD simulation results for S_L/S_T in Table VI. The result $S_L/S_T = 0.029$ for MD2 agrees with the experimental result, while $S_L/S_T = 0.035$ for MD1 does not. The MD simulation results are sensitive to the dipole moment of the model molecules, and the HRS measurement results indicate that the correct correlations are calculated by model MD2 which has molecular dipole moment close to the estimated liquid phase value. The best estimate for the dipole correlation strength parameter for acetonitrile is $a^3 = 6.29 \times 10^{-3} \text{ nm}^3$, the value for which the MD2 simulation gives S_L/S_T in exact agreement with the HRS result.

Equations (33)–(35) can be solved for ratios of the β tensor components. The β tensor components determine R^2 and P^2 , dipole correlations determine C_T and C_L , and both combined determine A_T/A_0 , I_{VV}/I_{HV} , and I_{HV}/I_{VH} . A particular solution for the acetonitrile β tensor is specified by giving three ratios of the nonvanishing independent Cartesian tensor components β_{zzz} , β_{zxx} , β_{xxz} , and β_{yyy} . There is a continuum of such solutions that exactly fit the HRS observations in Fig. 1 (e.g., using MD2, $C_T = 1.39$, $C_L = 0.041$, $\beta_{zxx}/\beta_{zzz} = 0.178$, $\beta_{xxz}/\beta_{zzz} = 0.171$, $\beta_{yyy}/\beta_{zzz} = -0.114$). *Ab initio* calculations of β tensor components for acetonitrile give $\beta_{zxx}/\beta_{zzz} = 0.021$ and $\beta_{yyy}/\beta_{zzz} = -0.136$ (Ref. 42, gas phase, static, electronic, CCSD [coupled cluster single double], t-aug-cc-pVTZ), $\beta_{xxz}/\beta_{zzz} = 0.117$ (Ref. 43, liquid, 1064 nm, CCSD(T) [perturbational triple], d-aug-cc-pVDZ), and $\beta_{zxx}/\beta_{zzz} = 0.132$, $\beta_{xxz}/\beta_{zzz} = 0.096$ (Ref. 44, liquid, 514.5 nm, MCSCF RAS [restricted active space]). Many β tensors with components similar to the ones from *ab initio* calculations fit the HRS observations for acetonitrile (using orientation correlations from the MD simulation). For DMSO, there is no solution of this type since dipole orientation correlation does not produce longitudinal HRS.

The HRS intensity is increased by the factor C_T due to orientation correlation, and the polarization and angle dependence for HRS is also modified by the long-range part of the orientation correlation. This has also been studied in several other liquids including water and nitrobenzene.^{5,7,9,33} The effect of the liquid environment on β itself has been investigated by QM calculations with reaction field models. Compared to the gas phase value, calculated $\beta_{||}$ is increased in liquid acetonitrile by a factor of 2.0 (Ref. 44, 514.5 nm, MCSCF RAS) or 3.0 (Ref. 43, 1064 nm, CCSD(T), d-aug-cc-pVDZ), and recent QM/Monte Carlo calculations for nitrobenzene solutions indicate further small changes in β when nearest neighbour orientation correlations are explicitly included.⁴⁵ The intermolecular interactions produce both orientation

correlation and molecular distortion. The HRS intensity for acetonitrile is increased by the factor C_T due to the correlations, further increased due to larger β for the distorted molecules in the liquid, and increased once more by the local field factors. The change in the HRS intensity due to the average molecular distortion is distinct from the HRS intensity change due to orientation correlation.

VI. COLLISION-INDUCED HRS

Slow fluctuation in molecular orientation is not the only motion contributing to the HRS signal measured in Fig. 1. A rapidly fluctuating increment $\Delta\beta$ is induced in each molecule during collisions with other molecules, and the resulting broad spectral component can also contribute to the measured HRS signal. The increment $\Delta\beta$ that is induced in one molecule, by the electric field of the permanent dipole, quadrupole, or octupole on a neighbouring molecule, is proportional to the second hyperpolarizability γ of the first molecule.^{10,11} The $\Delta\beta$ tensor resulting from the isotropic part of γ transforms as a vector, so a polar mode results from $\Delta\beta$ induced during intermolecular vibration and libration. It is usually assumed that the correlations for $\Delta\beta$ are short-range since the induction mechanism for $\Delta\beta$ is short-range.

Orientation and collision-induced (CI) HRS contributions can be distinguished spectroscopically (e.g., see HRS measurements and analysis for CDCl_3 in Ref. 13). Accordingly, the HRS spectrum previously measured for acetonitrile was decomposed into the sum of a narrow Lorentzian reorientation component ($[1 + (\Delta\nu/\nu_L)^2]^{-1}$ with $\nu_L = 1.68 \text{ cm}^{-1}$) and an overlapping broad exponential collision-induced component ($\exp[-|\Delta\nu/\nu_E|]$ with $\nu_E = 35 \text{ cm}^{-1}$).¹⁴ The respective integrated intensities of these components are 0.70 and 0.30 of the total for the HV HRS spectrum. The intensity ratio ($I_{\text{HV}}/I_{\text{VH}})_L$ measured for the Lorentzian components of the HV and VH spectra was 2.0, but the ratio was not measured for the exponential component. The single Lorentzian in the fit combines the two Lorentzians with widths in the ratio 1:6, due to the dipolar and octupolar parts of β , predicted by a simple rotational diffusion model.¹³ The HRS spectrum of DMSO has not been measured, but $\nu_L = 0.5 \text{ cm}^{-1}$ is estimated for the narrow Lorentzian component based on the measured 21.1 ps dielectric relaxation time.⁴⁶

The entire reorientation spectrum and part of the collision-induced spectrum are included in the 60 cm^{-1} measurement bandwidth (BW) used for most of the HRS measurements in the present work. The collision-induced contribution for $|\Delta\nu| > 30 \text{ cm}^{-1}$ can be separately determined from the difference in the HRS results obtained using filters with 60 and 336 cm^{-1} BW, as shown in Table III. The result of this measurement is that CI HRS is mainly transverse for acetonitrile (with $I_{\text{HV}}/I_{\text{VH}} = 1.46$) and CI HRS is mainly longitudinal for DMSO (with $I_{\text{HV}}/I_{\text{VH}} = 0.50$). This result is confirmed in Table IV by grating spectrometer measurements for a narrow band at $\Delta\nu = 20 \text{ cm}^{-1}$, where the reorientation spectrum is weak compared to the CI spectrum, giving $I_{\text{HV}}/I_{\text{VH}} = 1.28$ for acetonitrile and 0.45 for DMSO. The DMSO measurement at $\Delta\nu = 0 \text{ cm}^{-1}$ with 2 cm^{-1} BW, which includes the reorientation

spectrum and excludes the CI spectrum, gives $I_{\text{HV}}/I_{\text{VH}} = 0.98 \pm 0.03$, which is consistent with $\theta_{\mu\beta} \approx 90^\circ$ and the near absence of long-range orientation correlation for vector β . The non-local longitudinal HRS contribution for DMSO appears to be entirely collision-induced. The result $I_{\text{VV}}/I_{\text{HV}} = 8.2$ at $\Delta\nu = 0 \text{ cm}^{-1}$ for DMSO in Table IV indicates that the vector part of β is dominant.

The HRS results for acetonitrile and DMSO show that the CI HRS is non-local and can be either transverse or longitudinal. The origin and functional form for the vector $\Delta\beta$ correlations are not known, but correlations for vector $\Delta\beta$ decreasing asymptotically as r^{-3} would produce HRS with the same form as given by Eqs. (1)–(4). Non-local transverse optical (TO) and longitudinal optical (LO) vibration modes have been previously observed by hyper-Raman scattering in crystals, glasses, and liquids.^{17–19} The non-local CI HRS modes observed here may be similar, with both TO and LO components, each with its own spectrum. Polar non-local modes mediated by CI $\Delta\beta$ also can be present for nonpolar and centrosymmetric molecules and may account for $I_{\text{HV}}/I_{\text{VH}} \neq 1$ observed for HRS from liquids such as C_2Cl_4 , C_6H_6 , and CS_2 .⁵

VII. ION-INDUCED HRS

The intensity of ion-induced HRS increases with ion concentration and saturates at high ion concentration. The ion concentration dependence of the ion-induced HRS intensity in Eq. (6) is derived using the Debye-Huckel theory for the ion correlations, and the resulting expression for the ionic strength parameter c_0 in Eq. (6) is¹⁵

$$c_0 = \frac{K^2 \epsilon_0 \epsilon_s k_B T}{2e^2}, \quad (36)$$

where K is the magnitude of the scattering wavevector, ϵ_0 is the vacuum permittivity, ϵ_s is the static relative dielectric constant, k_B is the Boltzmann constant, and e is the electronic charge. The scattering wavenumber K is given by⁹

$$K^2 = (4\pi/\lambda_0)^2 [(n_i - n_s)^2 + 4n_i n_s \sin^2(\theta_s/2)], \quad (37)$$

where λ_0 is the vacuum wavelength of the incident light and n_i , n_s are refractive indices at the incident and scattered light frequencies. The experimental results in Figs. 2(a) and 3(a) for the ion-induced HRS concentration dependence can be compared with the theoretical result for c_0 given by Eqs. (36) and (37), evaluated using the data in Table V.^{47–51} For the experiments in Figs. 2 and 3, $2\pi/K = 281.0 \text{ nm}$ at $\theta_s = 90^\circ$ for acetonitrile and $2\pi/K = 1252 \text{ nm}$ at $\theta_s = 16.6^\circ$ for DMSO-d6. The calculated value $c_0 = 21.2 \mu\text{M}$ for acetonitrile from Eq. (36) is in good agreement with the experimental value $c_0 = 21.1 \pm 0.5 \mu\text{M}$ determined from the fit in Fig. 2(a). The calculated value $c_0 = 1.38 \mu\text{M}$ for DMSO-d6 is used in the fit to the data shown in Fig. 3(a).

The width of the ion-induced HRS spectrum is determined by ion diffusion, increases with ion concentration, and is usually much narrower than the width of the reorientation and collision-induced HRS spectra. An expression for the width

of the Lorentzian ion-induced HRS spectrum is^{15,52}

$$\nu_L^i = \nu_K [x + 2 - (x + 1)/(x + 2)], \quad (38)$$

$$\nu_K = K^2 D / (2\pi), \quad (39)$$

where $x = c/c_0$, $D^{-1} = (D_1^{-1} + D_2^{-1})/2$, and D_1 (D_2) is the diffusion coefficient for ion species 1 (2). The results calculated using this expression can be compared to spectral widths experimentally determined from the spectra in Figs. 2(b) and 3(b). Diffusion coefficients determined from the limiting conductance for acetonitrile-electrolyte solutions²³ are 1.863 (2.759) $\times 10^{-9}$ $\text{m}^2 \text{s}^{-1}$ for Li^+ (ClO_4^-), which gives $D = 2.224$ ($\times 10^{-9}$ $\text{m}^2 \text{s}^{-1}$) and $\nu_K = 0.177$ MHz. The degree of dissociation is 0.96 for the 2.0 mM LiClO_4 -acetonitrile solution, so $c = 1.92$ mM, $x = 90.7$, and $\nu_L^i = 16.6$ MHz, in good agreement with 16.0 ± 0.6 MHz measured for the spectrum in Fig. 2(b). For DMSO, the diffusion coefficients determined from the limiting conductances for DMSO-electrolyte solutions²⁴ are 0.386 (0.652) $\times 10^{-9}$ $\text{m}^2 \text{s}^{-1}$ for K^+ (ClO_4^-), which gives $D = 0.485$ ($\times 10^{-9}$ $\text{m}^2 \text{s}^{-1}$) and $\nu_K = 1.95$ kHz. The 0.60 mM KClO_4 -DMSO solution is fully dissociated, so $c = 0.60$ mM, $x = 433$, and $\nu_L^i = 0.85$ MHz, in good agreement with 0.84 ± 0.17 MHz measured for the spectrum in Fig. 3(b).

Figure 2 shows two complementary measurements of the ion-induced HRS contribution for acetonitrile, the first using $I_{\text{HV}}/I_{\text{VH}}$ versus ionic strength in Fig. 2(a) and the second using a high resolution VH HRS spectrum in Fig. 2(b). The relative ion-induced contribution 0.88 ± 0.04 in Fig. 2(b) is given by the ratio of the integrated intensity of the ion-induced HRS peak to the integrated intensity of the flat background due to intrinsic HRS. This result from Fig. 2(b) is in good agreement with the relative contribution $Bx/(1+x) = 0.90$ calculated from the fit in Fig. 2(a). Ion-induced HRS is much weaker for DMSO-d6, so Fig. 3(b) shows the spectrum for HH HRS which is more intense than VH HRS by a factor about R^2 at $\theta_s = 16.6^\circ$. The HH integrated intensity ratio is 0.0630 ± 0.0014 for the ion-induced HRS peak to intrinsic HRS background in Fig. 3(b). Using this result, with Eqs. (7) and (8) and the intrinsic HRS results from Fig. 1(b), one obtains $B = 0.0533$ at $\theta_s = 16.6^\circ$, which is used in the fit to $I_{\text{HV}}/I_{\text{VH}}$ shown in Fig. 3(a), and also $B = 0.0367$ at $\theta_s = 90^\circ$.

The parameter $B = (I_{\text{VH}}^i)_{c \rightarrow \infty} / (I_{\text{VH}})_{c=0} = I_{\text{VH},\infty}^i / I_{\text{VH},0}$ in Eq. (6) is a measure of the maximum ion-induced HRS intensity relative to the intrinsic HRS intensity. The ion-induced HRS intensities are given by¹⁵

$$I_{\text{VV}}^i = I_{\text{HV}}^i = 0, \quad (40)$$

$$I_{\text{VH}}^i = C \rho^2 \left(\frac{k_B T}{\epsilon_0 \epsilon_s} \right) \left(\gamma_{\perp} + \frac{\mu \beta_{\perp}}{3k_B T} \right)^2 f(0)^2 \frac{K_D^2}{K^2 + K_D^2} \cos^2(\theta_s/2), \quad (41)$$

$$I_{\text{HH}}^i = I_{\text{VH}}^i [1 + (R - 1) \cos \theta_s]^2, \quad (42)$$

where

$$K_D^2 = \frac{2ce^2}{\epsilon_0 \epsilon_s k_B T} \quad (43)$$

is the Debye-Huckel screening parameter, c is the ionic strength, $f(0) = \epsilon_s(\epsilon_{\infty} + 2)/(\epsilon_{\infty} + 2\epsilon_s)$ is the Onsager local field factor, $\beta_{\perp} = (1/5) \sum_{\alpha} (2\beta_{2\alpha\alpha} - \beta_{\alpha\alpha z})$,

$\gamma_{\perp} = (1/15) \sum_{\alpha\beta} (2\gamma_{\alpha\beta\beta\alpha} - \gamma_{\alpha\alpha\beta\beta})$, $\gamma_{\alpha\beta\gamma\delta}(-2\omega; 0, \omega, \omega)$ is the second hyperpolarizability,⁵³ and the factor C includes all other geometric, optical field, and instrumental factors.

A simple expression is obtained for B at $\theta_s = 90^\circ$ in the case that there are no intrinsic orientation correlations, Kleinman symmetry applies, $\theta_{\mu\beta} = 0$, and both γ and octupolar β are negligible so that $I_{\text{VH}} = (1/45) |\beta^{[\text{ss},1]}|^2 = \langle \beta_{\text{ZZZ}}^2 \rangle$ and $\beta_{\perp}^2 / \langle \beta_{\text{ZZZ}}^2 \rangle = 3$. The expression is

$$B_0 = 3f(0)^2 y / (2\epsilon_s), \quad (44)$$

where y is the dimensionless dipole strength given by Eq. (14). Table V shows calculated B_0 values which are $2.4\times$ and $37\times$ the respective experimental B values for acetonitrile and DMSO.

A better theoretical estimate for B is obtained by including the effects of γ , orientation correlation, and collision-induced HRS. Including γ increases the ion-induced intensity $I_{\text{VH},\infty}^i$ for acetonitrile by the factor $[1 + 3k_B T \gamma_{\perp} / (\mu \beta_{\perp})]^2 = 1.23$, calculated using the *ab initio* results $\mu = 4.59$ D, $\beta_{\parallel} = 67.7$ au, and $\gamma_{\parallel} = 4776$ au for liquid phase ESHG at $\lambda = 1064$ nm.⁴³ Including orientation correlations increases $I_{\text{VH},0}$ by a factor $C_T = 1.4$, and including collision-induced HRS increases $I_{\text{VH},0}$ by a further factor $1/0.70$. The revised estimate is then $B = 1.35$, which is still $1.5\times$ larger than the experimental value for acetonitrile. Quantitative agreement is not obtained for B , which may be due to uncertainties in the parameters entering the calculation and also due to theoretical uncertainty about the Onsager local field factor in Eq. (41). For DMSO, the difference between B_0 and measured B is mainly due to the large angle $\theta_{\mu\beta}$ between μ and vector β , which reduces B by the factor $\cos^2 \theta_{\mu\beta}$. Neglecting γ , orientation correlation, octupolar β , and collision-induced HRS, and fitting $B_0 \cos^2 \theta_{\mu\beta}$ to the experimental value $B = 0.0367$, one obtains $\theta_{\mu\beta} = 99.5^\circ$. Including γ will increase the estimated angle $\theta_{\mu\beta}$ since $I_{\text{VH},\infty}^i$ is decreased by the cancellation of the γ and $\mu\beta$ terms in Eq. (41), which have opposite sign for DMSO.^{39,40}

There are several sources of uncertainty for the ion-induced HRS intensity. The Onsager local field factor in Eq. (41) expresses the relation between the macroscopic electric field of the ions and the microscopic field that orients and distorts the molecules. Although the Onsager local field factor is commonly used, its accuracy is uncertain. An independent determination of the local field factor by ion-induced HRS may be possible⁹ and could have implications for surface studies that use second harmonic generation as a probe.⁵⁴ The ion-induced HRS intensity is measured relative to the intrinsic HRS for ion-free liquids. The relative intensity of ion-induced HRS and reorientation HRS due to just vector β , given by Eq. (44), is a simple expression where the poorly known hyperpolarizabilities cancel out, but this expression omits several contributions that are too large to ignore. The intrinsic HRS intensity is the sum of several different overlapping components, and additional spectral measurements and analysis are needed to disentangle the components and express them in terms of the vector β HRS contribution. Ion-induced HRS also has a significant contribution from γ in polar liquids. In non-polar liquids, ion-induced HRS is entirely due to γ , but in this case the intensity will be limited by the low

solubility and dissociation of ionic compounds in non-polar solvents.

VIII. LONG RANGE CORRELATION

Orientation correlations for homogeneous, isotropic, random vector fields have been considered in this work and are described by the orientation correlation functions $B_L(r)$ and $B_T(r)$. Coherent HRS contributions from $\beta^{(1)}$ are directly related to the spectral functions $S_T(K)$ and $S_L(K)$ given by Eqs. (19) and (20), obtained from the Fourier transform of the correlation tensor. The coefficients A_T and A_L for the fits to the HRS data in Fig. 1 are constants, independent of scattering wavevector magnitude $K \propto \sin(\theta_s/2)$, and this observation places a strong constraint on the possible correlation functions. Spectral functions $S_T \neq S_L$ which are slowly varying near $K = 0$, and constant coefficients $A_T \neq A_L$ in Eqs. (1)–(4), are the result of correlation functions B_L and B_T with r^{-3} long range asymptotic form.⁸

Ion-induced HRS in the limit of low ionic strength, which is governed by radial orientation correlation with r^{-2} asymptotic form at long range, gives a different result. In this case, the orientation vector field is not homogeneous since it is radial around each isolated ion. Equations (40)–(43) can be put in the form of Eqs. (1)–(4) with $A_0 = A_T = 0$, but with $A_L \propto K^{-2}$ when $c \rightarrow 0$.

For ion-induced HRS at high ionic strength, the field of the screened ions becomes homogeneous and the coefficient $A_L \propto S_L(K) \propto (K^2 + K_D^2)^{-1}$ given by Eq. (41) tends to a constant. In this case, the orientation correlation function obtained from the inverse Fourier transform of $S_L(K) \propto (K^2 + K_D^2)^{-1}$ and $S_T(K) = 0$ is

$$B_T(r) \propto [1 - (1 + K_D r) \exp(-K_D r)]/r^3, \quad (45)$$

$$B_L(r) = B_T(r) + r dB_T(r)/dr. \quad (46)$$

At high ionic strength and at long range such that $K_D r \gg 1$, the correlation function has r^{-3} long-range asymptotic form.

The presence of correlations with r^{-3} long range asymptotic form is indicated by HRS data, such as that in Fig. 1, which is fit by Eqs. (1)–(4) with constant coefficients $A_T \neq A_L$. Longitudinal HRS with $A_T < A_L$ is observed for DMSO-d6 and is entirely due to the collision-induced HRS contribution. This indicates that collision-induced $\Delta\beta$ for DMSO has long-range correlation with r^{-3} asymptotic form. Dipole interaction for collision-induced polar modes of intermolecular vibration and libration may be the source of the long-range correlation, but contrary to the observation that dipole-dipole orientation correlation gives only transverse orientation HRS, the HRS contribution for collision-induced modes may be either transverse (acetonitrile) or longitudinal (DMSO). Contributions from correlated molecules up to at least $r = \pi/K$ must be included to observe $A_T \neq A_L$, so the correlations between molecules over distances $r > 100$ nm are required to account for the HRS observations.³³

IX. SUMMARY AND CONCLUSION

The HRS results for acetonitrile and DMSO illustrate the main features present in the HRS spectra of a pure liquid. HRS

is often thought of as incoherent second harmonic light scattering from randomly oriented, uncorrelated, and undistorted molecules. The spectral component due to molecular reorientation most closely matches this picture, but this contribution is modified by the effect of both short-range and long-range molecular orientation correlations and by the average distortion of the molecule by its environment. The long-range correlation due to the dipole-dipole interactions in a polar liquid acting on the first rank irreducible (vector) part of the molecular first hyperpolarizability tensor β results in a transverse HRS spectrum, with a clear observational signature in its polarization and angle dependence. The intensity of the coherent HRS contribution depends on the size of the vector and octupolar parts of β and on the angle between vector β and the molecular dipole vector. The spectral width of the reorientation HRS component is typically 0.1 – 10 cm^{-1} , inversely proportional to the orientation relaxation time for molecules in the liquid. This is often but not always the most intense HRS contribution. Although it is often the goal, there is usually not enough information in the HRS measurements to uniquely determine the β tensor components for the molecule. However, the long-range dipole correlation strength a^3 can be precisely determined from combined MD and reorientation HRS results.

The fluctuating environment for each molecule results in a distortion of the molecule which fluctuates on the collision time scale. An increment $\Delta\beta \propto \gamma E$ is induced by the multipole electric field E of the neighbouring molecules acting on the molecular second hyperpolarizability γ , and the intensity of collision-induced HRS due to $\Delta\beta$ can be comparable to the intensity of HRS due to β . The multipole field varies rapidly in space, so the increment $\Delta\beta$ also varies rapidly in time during molecular collisions, producing a broad HRS spectrum with typical width 10 – 100 cm^{-1} . Explicit calculation of $\Delta\beta$ using MD simulation has recently become feasible and may lead to quantitative calculations of CI HRS.⁵⁵ The increment $\Delta\beta \propto \gamma E$ has a part that transforms as a vector, so the intermolecular vibrations and librations associated with $\Delta\beta$ are polar modes. The observed polarization dependence for collision-induced HRS shows that these modes are non-local and that they can be either transverse or longitudinal. Analogous to the hyper-Raman scattering observations seen for intra-molecular vibrations, each mode may be split into transverse and longitudinal components with different spectra. The correlation function for $\Delta\beta$ appears to have r^{-3} long-range asymptotic form.

The third distinct HRS component is induced by the electric field of dissolved ions. The ion field orients the dipoles, correlates β , and induces correlated $\Delta\beta$ on the surrounding molecules. Coherent second harmonic light scattering by these molecules is the result of the correlations. In a dilute electrolyte solution, most molecules are far from the ions, so the net electric field seen by a molecule varies slowly in time as the ions diffuse through the liquid. The resulting HRS spectrum is narrow, typically 10^{-6} – 10^{-3} cm^{-1} . The intensity of ion-induced HRS increases with ion concentration, saturating at a maximum intensity comparable to the other two HRS contributions, at ionic strength above about 0.1 mM. Theoretical predictions for the ion concentration dependence

of the intensity and spectral width are in quantitative agreement with the experiment for ion-induced HRS. However, the result of the comparison of theory and experiment for the ion-induced HRS intensity is less satisfactory and more uncertain.

SUPPLEMENTARY MATERIAL

See [supplementary material](#) for details about the molecular dynamics simulation models for acetonitrile and DMSO.

ACKNOWLEDGMENTS

This work was supported by the National Science Foundation (NSF) through Grant No. CHE-1212114.

- ¹J. Campo, F. Desmet, W. Wenseleers, and E. Goovaerts, *Opt. Express* **17**, 4587 (2009).
- ²K. Clays and A. Persoons, *Phys. Rev. Lett.* **66**, 2980 (1991).
- ³L.-T. Cheng, W. Tam, S. H. Stevenson, G. R. Meredith, G. Rikken, and S. R. Marder, *J. Phys. Chem.* **95**, 10631 (1991).
- ⁴D. P. Shelton, *J. Opt. Soc. Am. B* **17**, 2032 (2000); Erratum, **34**, 1550 (2017).
- ⁵D. P. Shelton, *J. Chem. Phys.* **136**, 044503 (2012).
- ⁶D. P. Shelton, *J. Chem. Phys.* **138**, 154502 (2013).
- ⁷D. P. Shelton, *J. Chem. Phys.* **141**, 224506 (2014).
- ⁸D. P. Shelton, *J. Chem. Phys.* **143**, 134503 (2015); Erratum, **146**, 199901 (2017).
- ⁹D. P. Shelton, *J. Chem. Phys.* **144**, 234506 (2016).
- ¹⁰S. Kielich, *Phys. Lett. A* **27**, 307 (1968).
- ¹¹S. Kielich, J. R. Lalanne, and F. B. Martin, *Phys. Rev. Lett.* **26**, 1295 (1971).
- ¹²P. Kaatz and D. P. Shelton, *Mol. Phys.* **88**, 683 (1996).
- ¹³P. Kaatz and D. P. Shelton, *Opt. Commun.* **157**, 177 (1998).
- ¹⁴D. P. Shelton, *J. Chem. Phys.* **123**, 084502 (2005).
- ¹⁵D. P. Shelton, *J. Chem. Phys.* **130**, 114501 (2009).
- ¹⁶D. P. Shelton, *J. Chem. Phys.* **138**, 054502 (2013).
- ¹⁷V. N. Denisov, B. N. Mavrin, V. B. Podobedov, and Kh. E. Sterin, *Sov. Phys. JETP* **57**, 733 (1983).
- ¹⁸V. N. Denisov, B. N. Mavrin, and V. B. Podobedov, *Phys. Rep.* **151**, 1 (1987).
- ¹⁹V. Rodriguez, *J. Raman Spectrosc.* **43**, 627 (2012).
- ²⁰D. P. Shelton, *J. Chem. Phys.* **132**, 154506 (2010).
- ²¹D. P. Shelton, *Rev. Sci. Instrum.* **82**, 113103 (2011).
- ²²D. P. Shelton, W. M. O'Donnell, and J. L. Norton, *Rev. Sci. Instrum.* **82**, 036103 (2011).
- ²³J. Barthel, L. Iberl, J. Rossmairer, H. J. Gores, and B. Kaukal, *J. Solution Chem.* **19**, 321 (1990).
- ²⁴C. Atlani and J.-C. Justice, *J. Solution Chem.* **4**, 955 (1975).
- ²⁵L. Yu and B. S. Rawat, *J. Lightwave Technol.* **10**, 556 (1992).
- ²⁶Y. Zhan, Q. Yang, H. Wu, J. Lei, and P. Liang, *Optik* **120**, 585 (2009).
- ²⁷P. Kaatz and D. P. Shelton, *J. Chem. Phys.* **105**, 3918 (1996).
- ²⁸P. Kaatz, E. A. Donley, and D. P. Shelton, *J. Chem. Phys.* **108**, 849 (1998).
- ²⁹M. J. Abraham, D. van der Spoel, E. Lindahl, B. Hess, and GRO-MACS Development Team, GROMACS User Manual version 5.1.4, www.gromacs.org (2016).
- ³⁰M. Shirts, D. L. Mobley, J. D. Chodera, and V. S. Pande, *J. Phys. Chem B* **111**, 13052 (2007).
- ³¹G. Bussi, D. Donadio, and M. Parrinello, *J. Chem. Phys.* **126**, 014101 (2007).
- ³²C. Zhang and G. Galli, *J. Chem. Phys.* **141**, 084504 (2014).
- ³³D. P. Shelton, *J. Chem. Phys.* **147**, 154501 (2017).
- ³⁴V. Ballenegger and J.-P. Hansen, *Mol. Phys.* **102**, 599 (2004).
- ³⁵J. M. Caillol, *J. Chem. Phys.* **96**, 7039 (1992).
- ³⁶R. Rivelino, B. J. C. Cabral, K. Coutinho, and S. Canuto, *Chem. Phys. Lett.* **407**, 13 (2005).
- ³⁷T. Ohba and S. Ikawa, *Mol. Phys.* **73**, 985 (1991).
- ³⁸J. M. M. Cordeiro and A. K. Soper, *J. Chem. Phys.* **138**, 044502 (2013).
- ³⁹I. Ledoux and J. Zyss, *Chem. Phys.* **73**, 203 (1982).
- ⁴⁰D. N. Rao, N. K. M. N. Srinivas, P. Gangopadhyay, and T. P. Radhakrishnan, *J. Phys. Chem. A* **108**, 5213 (2004).
- ⁴¹P. D. Maker, *Phys. Rev. A* **1**, 923 (1970).
- ⁴²J. R. Hammond and K. Kowalski, *J. Chem. Phys.* **130**, 194108 (2009).
- ⁴³H. Reis, M. G. Papadopoulos, and A. Avramopoulos, *J. Phys. Chem. A* **107**, 3907 (2003).
- ⁴⁴P. Norman, Y. Luo, and H. Agren, *J. Chem. Phys.* **107**, 9535 (1997).
- ⁴⁵M. H. Cardenuto and B. Champagne, *J. Chem. Phys.* **141**, 234104 (2014).
- ⁴⁶U. Kaatz, R. Pottel, and M. Schafer, *J. Phys. Chem.* **93**, 5623 (1989).
- ⁴⁷D. P. Shelton, *Appl. Opt.* **50**, 4091 (2011).
- ⁴⁸K. Moutzouris, M. Papamichael, S. C. Betsis, I. Stavrakas, G. Hloupis, and D. Triantis, *Appl. Phys. B* **116**, 617 (2014).
- ⁴⁹I. Z. Kozma, P. Krok, and E. Riedle, *J. Opt. Soc. Am. B* **22**, 1479 (2005).
- ⁵⁰A. Stoppa, A. Nazet, R. Buchner, A. Thoman, and M. Walther, *J. Mol. Liquids* **212**, 963 (2015).
- ⁵¹J. Barthel and R. Buchner, *Pure Appl. Chem.* **63**, 1473 (1991).
- ⁵²B. J. Berne and R. Pecora, in *Dynamic Light Scattering* (Wiley, New York 1976), Chap. 13.
- ⁵³D. P. Shelton and J. E. Rice, *Chem. Rev.* **94**, 3 (1994).
- ⁵⁴G. Gonella, C. Lutgebaucks, A. G. F. de Beer, and S. Roke, *J. Phys. Chem. C* **120**, 9165 (2016).
- ⁵⁵C. Liang, G. Tocci, D. M. Wilkins, A. Grisafi, S. Roke, and M. Ceriotti, *Phys. Rev. B* **96**, 041407(R) (2017).